EACS 2016 – 6th European Conference on Structural Control Sheffield, England: 11-13 July 2016
Paper No. 113

OPTIMAL DESIGN AND PRACTICAL IMPLEMENTATION OF EDDY-CURRENT TUNED MASS DAMPERS WITH PERMANENT MAGNETS FOR MULTI-STOREY BUILDINGS

Álvaro Magdaleno[1], Emiliano Pereira[2], Javier Castaño[3], Norberto Ibán[3], Iván M. Díaz[4] & Antolín Lorenzana,[1]

[1]ITAP, EII, Universidad de Valladolid, 47011, Valladolid, Spain
[2]EPS, Universidad de Alcalá, 28805, Alcalá de Henares (Madrid), Spain
[3]Centro Tecnológico CARTIF, 47151, Boecillo (Valladolid), Spain
[4]ETSICCP, Universidad Politécnica de Madrid, 28040, Madrid, Spain

Corresponding author: Emiliano.Pereira@uah.es

ABSTRACT. This work proposes an implementation example of two tuned mass dampers (TDM) on a reduced scale two storey building. The TMD, in which the damping is magnetically adjusted without contact, is a laboratory prototype built in CARTIF (Spain). This TMD consists on a one degree of freedom system formed by a permanent magnet (mass) fixed to a flexible link (elasticity) and an aluminium plate at an adjustable distance to the magnet (damping). The tuning of the TMDs is carried out by considering the passive system as a feedback controller. The system identification and the experimental results show the validity of theoretical approximations and the design criterions.

KEYWORDS: Structural control, Passive vibration control, Tuned mass damper, Optimization.

1 INTRODUCTION

Structures subjected to excitations like earthquake ground motions, human induced vibrations or machinery may produce structural damages (or even collapse) and serviceability limit state problems. Passive, semi-active and active vibration controls have been proposed as possible solutions to reduce the vibration level at civil structures such as bridges, multi-storey buildings or slender floor structures, among others [1].

Tuned Mass Dampers (TMD), which can be used for passive and semi-active control strategies, improves the vibration response of a structure by increasing its damping (i.e. energy dissipation) and/or stiffness (i.e. energy storage) through the application of forces generated in response to the movement of the structure [2]. Recently, different TMD implementations have been proposed in order to improve the tuning of mechanical parameters. For example, magnetic TMDs have been used due to its linear behaviour and since its damping coefficient can be easily and finely calibrated [3, 4]. A pendulum with an adjustable length is used to tune the resonance of a Smart TMD in [5], which is used for a semi-active control strategy. Other example is found at [6], where a TMD based on shape memory alloys and eddy currents is utilized for implementing two adaptive control strategies. In the case of structures with spatially distributed and closely spaced natural frequencies, the TMD design may not be obvious because Den Hartog's theory [7] may not be applied due to the existence of a coupling between the motions of the

vibration modes of the structures and the used TMD's [8]. Multi storey buildings are good examples of structures with spatially distributed and closely spaced natural frequencies. For example, Greco et al. [9] propose a robust optimum design of tuned mass dampers installed on multi-degree-of-freedom systems subjected to stochastic seismic actions. The robust design is formulated as a multi-objective optimization problem, in which both the mean and the standard deviation of the performance index are simultaneously minimized. Other similar examples can be found at [10] and [11]; however, simulation results are only presented in aforementioned references.

In this work, a system composed of two magnetic TDM devices based on a cantilever beam are implemented in a reduced scale two floor building [12]. The tuning of the TMD parameters is carried out by considering this passive vibration control (PVC) from the active vibration (AVC) control point of view (see reference [13]). This simplifies the design of this PVC because the coupling between the two main vibration modes is not a problem (as in Den Hartog's theory). In addition, this work designs and implements a magnetic TDM tuning based on minimizing the H_∞ norm of the frequency response function (FRF) between the acceleration of the second floor and the acceleration of the ground. Simulation and experimental results are obtained to show: i) the advantages of a magnetic TMD which can be easy tuned after an experimental identification, ii) the validation of the model approximations for magnetic TMDs and iii) the design of TMDs can be carried out from and AVC point of view, which is an advantage compared with Den Hartog's theory for structures with natural frequencies spatially distributed and closely spaced.

2 MODELING AND EXPERIMENTAL IDENTIFICATION

The generalized framework to design robust TMD proposed in [13] is considered in this work. This framework is simplified and particularized to a two storey building, which makes the explanation easier to follow than [13] for this particular application.

The model of the magnetic TMD's is considered as [3], i.e. drag forces provided by magnetic dampers are assumed to be proportional to velocity. This assumption is demonstrated with experimental identification of the linear and time invariant model.

Fig. 1 right shows the magnetic TMD prototypes used in this work. Note that these TMD's can be fixed to the two storey building with the structure (4). The magnetic TMD is tuned as follows: i) the rigidity is changed by the link (1), ii) the mass is varied by adding standard hex nuts to the magnet (2) and iii) damping is configured by moving the plate (3) with respect to the magnet (2).

2.1 Two storey building

The two storey building can be modelled as a two degree of freedom system (see Fig. (2) left), where the mass is concentrated at each floor (m_1 and m_2), k_1 and c_1 are, respectively, the first floor stiffness and damping coefficient (relative to the ground) and k_2 and c_2 are, respectively, the second floor linear stiffness and damping coefficient (relative to the first floor).

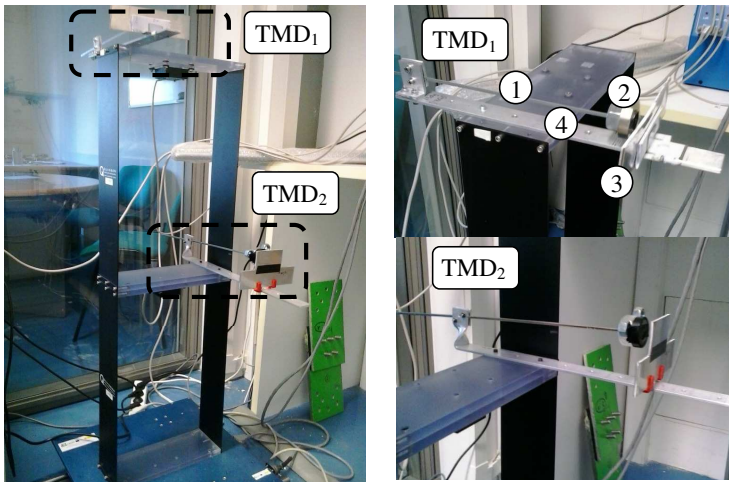

Figure 1: Two storey building (left) and details for the magnetic TMDs (right).

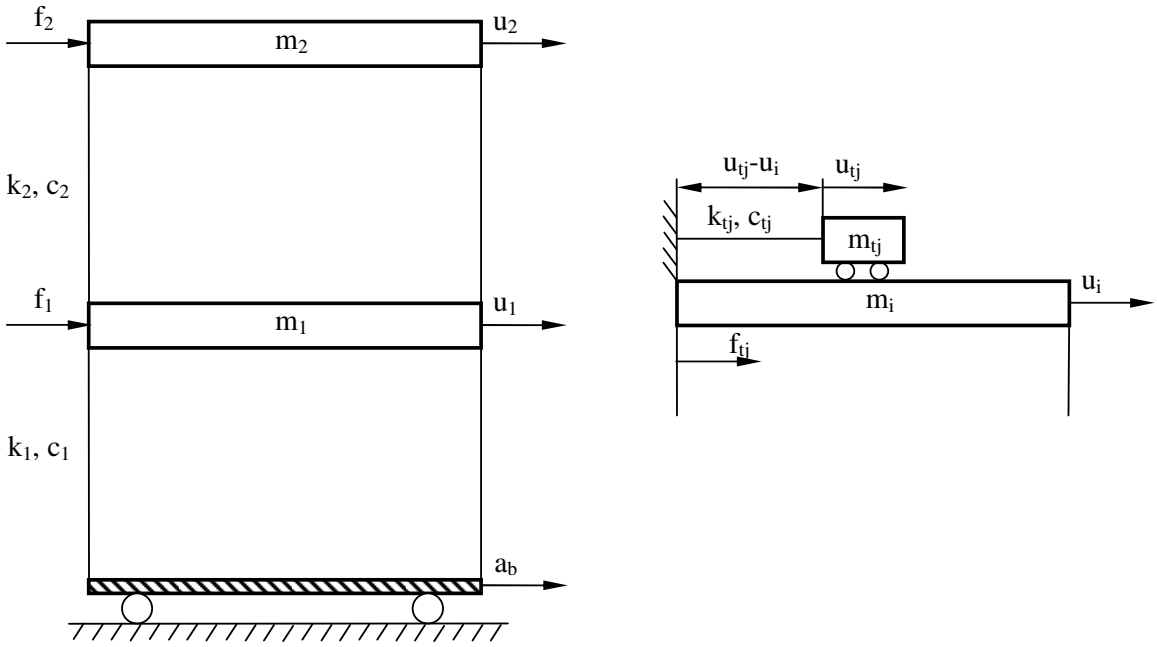

Figure 2: Two storey building (left) and TMD (right) models.

If the applied forces in each floor (f_1 and f_2) and the acceleration of the base (a_b) are considered as inputs, the differential equation of the building can be represented as follows:

$$\mathbf{M\ddot{u}} + \mathbf{C\dot{u}} + \mathbf{Ku} = -\mathbf{M}\begin{bmatrix} a_b \\ a_b \end{bmatrix} + \mathbf{f}, \tag{1}$$

where

$$\mathbf{M} = \begin{bmatrix} m_1 & 0 \\ 0 & m_2 \end{bmatrix},\ \mathbf{C} = \begin{bmatrix} c_1 + c_2 & -c_2 \\ -c_2 & c_2 \end{bmatrix},\ \mathbf{K} = \begin{bmatrix} k_1 + k_2 & -k_2 \\ -k_2 & k_2 \end{bmatrix}, \mathbf{u} = \begin{bmatrix} u_1 \\ u_2 \end{bmatrix},\ \mathbf{f} = \begin{bmatrix} f_1 \\ f_2 \end{bmatrix}, \tag{2}$$

This model considers nodal coordinates or real displacements. This system can be represented in modal coordinates by obtaining the eigenvectors (mode shapes) and eigenvalues (natural frequencies):

$$\left(-\omega_i^2\mathbf{M} + \mathbf{K}\right)\boldsymbol{\phi_i} = 0, \tag{3}$$

where the eigenvectors can be grouped in the following matrix:

$$\mathbf{\Phi} = \begin{bmatrix} \boldsymbol{\phi}_1 & \boldsymbol{\phi}_2 \end{bmatrix} = \begin{bmatrix} \phi_{11} & \phi_{21} \\ \phi_{12} & \phi_{22} \end{bmatrix}, \tag{4}$$

where $\phi_i j$ is the j^{th} component of the i^{th} mode shape. The relationship between nodal and modal coordinates is $\boldsymbol{u} = \mathbf{\Phi}\boldsymbol{\eta}$. Then, after having pre-multiplied by $\mathbf{\Phi}^T$ in order to uncouple the equation system, Eq. (1) in modal coordinates is

$$\mathbf{\Phi}^T\mathbf{M\Phi}\ddot{\boldsymbol{\eta}} + \mathbf{\Phi}^T\mathbf{C\Phi}\dot{\boldsymbol{\eta}} + \mathbf{\Phi}^T\mathbf{K\Phi}\eta = -\mathbf{\Phi}^T\mathbf{M}\begin{bmatrix} a_b \\ a_b \end{bmatrix} + \mathbf{\Phi}^T\mathbf{f}, \tag{5}$$

The state space state model can be deduced from Eq. (5) by taking, as the state-space variables, the modal coordinates ($\boldsymbol{\eta}$) and their first derivatives ($\dot{\boldsymbol{\eta}}$). Thus, if $\mathbf{\Phi}^T\mathbf{M\Phi} = \tilde{\mathbf{M}}$, $\mathbf{\Phi}^T\mathbf{C\Phi} = \tilde{\mathbf{C}}$ and $\mathbf{\Phi}^T\mathbf{K\Phi} = \tilde{\mathbf{K}}$, the linear differential equation of the state space vector is

$$\begin{bmatrix} \dot{\boldsymbol{\eta}} \\ \ddot{\boldsymbol{\eta}} \end{bmatrix} = \begin{bmatrix} \mathbf{0}_{2,2} & \boldsymbol{I}_2 \\ -\tilde{\mathbf{M}}^{-1}\tilde{\mathbf{K}} & -\tilde{\mathbf{M}}^{-1}\tilde{\mathbf{C}} \end{bmatrix}\begin{bmatrix} \boldsymbol{\eta} \\ \dot{\boldsymbol{\eta}} \end{bmatrix} - \begin{bmatrix} \mathbf{0}_{2,2} \\ \tilde{\mathbf{M}}^{-1}\mathbf{\Phi}^T\mathbf{M} \end{bmatrix}\begin{bmatrix} a_b \\ a_b \end{bmatrix} + \begin{bmatrix} \mathbf{0}_{2,2} \\ \tilde{\mathbf{M}}^{-1}\mathbf{\Phi}^T \end{bmatrix}\mathbf{f}, \tag{6}$$

and the output equation is

$$\begin{bmatrix} \mathbf{y}_1 \\ \mathbf{y}_2 \end{bmatrix} = \begin{bmatrix} \ddot{\mathbf{u}}_1 \\ \ddot{\mathbf{u}}_2 \end{bmatrix} + \begin{bmatrix} a_b \\ a_b \end{bmatrix} = \begin{bmatrix} -\mathbf{\Phi}\tilde{\mathbf{M}}^{-1}\tilde{\mathbf{K}} & -\mathbf{\Phi}\tilde{\mathbf{M}}^{-1}\tilde{\mathbf{C}} \end{bmatrix}\begin{bmatrix} \dot{\boldsymbol{\eta}} \\ \ddot{\boldsymbol{\eta}} \end{bmatrix} + \mathbf{\Phi}\tilde{\mathbf{M}}^{-1}\mathbf{\Phi}^T\mathbf{f}, \tag{7}$$

where $\mathbf{\Phi}\tilde{\mathbf{M}}^{-1}\mathbf{\Phi}^T\mathbf{M} = \mathbf{I}_2$ and

$$\tilde{\mathbf{M}}^{-1} = \mathbf{I}_2,\ \tilde{\mathbf{K}} = \begin{bmatrix} \omega_1^2 & 0 \\ 0 & \omega_2^2 \end{bmatrix},\ \tilde{\mathbf{C}} = \begin{bmatrix} 2\xi_1\omega_1 & 0 \\ 0 & 2\xi_2\omega_2 \end{bmatrix}. \tag{8}$$

Note that y_1 and y_2 are accelerations that can be measured with accelerometers mounted at first and second floor, respectively.

Once the system model is established, the following step is the experimental identification. A chirp signal between 0.5 Hz and 15 Hz with a duration of 300 seconds was applied to the base of the structure (a_b). The FRF of the system, where H_2 mode is considered, and the FRF of the model adjusted by minimizing the means square error is shown at Figs. (3) and (4).

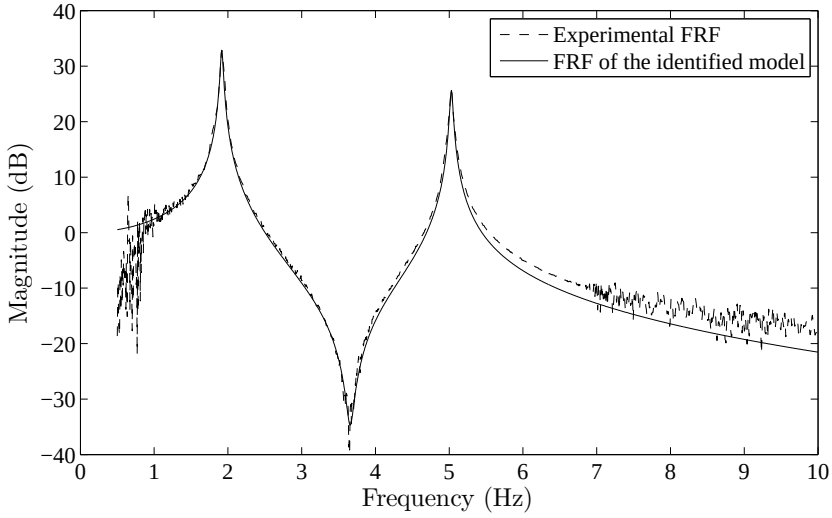

Figure 3: Structure identification example (first floor).

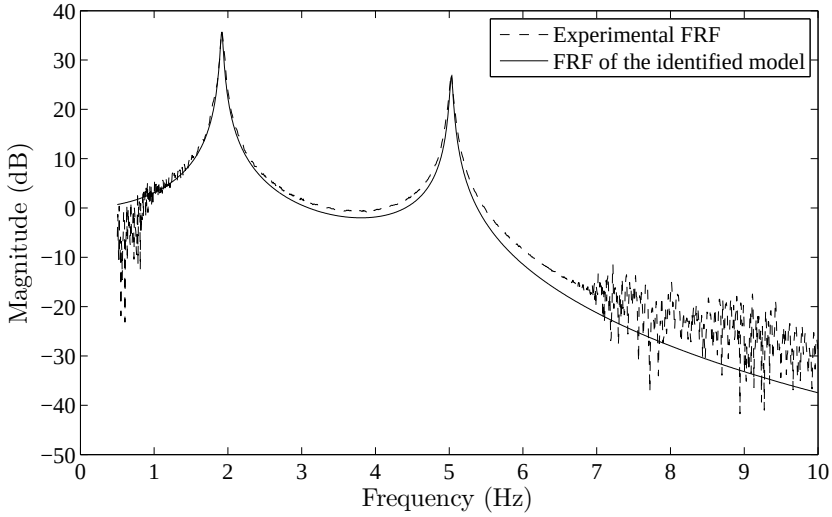

Figure 4: Structure identification example (second floor).

2.2 Magnetically damped TMD

The TMD can be modelled as a one degree of freedom system (see Fig. (2) right), where m_{tj} is the mass, k_{tj} and c_{tj} are the TMD linear stiffness and damping coefficient of the j^{th} TMD relative to the i^{th} floor.

If the accelerations of the base (a_b) and i^{th} floor are considered as inputs, the differential equation of the TMD can be represented as follows:

$$m_{t,j}\ddot{u}_{tj} + c_{t,j}\dot{u}_{t,j} + k_{t,j}u_{t,j} - c_{t,j}u_i - k_{t,j}u_i = -m_{t,j}a_b. \tag{9}$$

The force applied by the TMD to the i^{th} floor is:

$$f_{t,j} = k_{t,j}\left(u_{t,j} - u_i\right) + c_{t,j}\left(\dot{u}_{t,j} - \dot{u}_i\right) = k_{t,j}u_{r,ij} + c_{t,j}\dot{u}_{r,ij}. \tag{10}$$

If the relative displacement between j^{th} TMD and i^{th} floor is defined as $u_{r,ij} = u_{t,j} - u_i$, the transfer function between the acceleration measured by an accelerometer placed at i^{th} floor (denoted above as y_i) and $u_{r,ij}$ from Eq. (9) is as follows:

$$U_{r,ij}(s) = -\frac{m_{t,j}}{m_{t,j}s^2 + c_{t,j}s + k_{t,j}}Y_i(s). \tag{11}$$

Therefore, from Eqs. (10) and (11) can be deduced the following transfer function of the TMD

$$F_{t,j}(s) = -\frac{m_{t,j}\left(c_{t,j}s + k_{t,j}\right)}{m_{t,j}s^2 + c_{t,j}s + k_{t,j}}Y_i(s) = m_{t,j}\frac{2\xi_{t,j}\omega_{t,j}s + \omega_{t,j}^2}{s^2 + 2\xi_{t,j}\omega_{t,j}s + \omega_{t,j}^2}Y_i(s), \tag{12}$$

where $\omega_{t,j}$ and $\xi_{t,j}$ are, respectively, the natural frequency and damping ratio of the j^{th} TMD as an isolated system.

The linear time invariant (LTI) model defined in Eq. (12) is identified by obtaining the initial conditions and the values of $\omega_{t,j}$ and $\xi_{t,j}$ that minimizing the least square error of an impact response. An example of the input signal considered in the system identification is shown at Fig. 5. Note that only the interval from 0.5 to 1.2 seconds is used for the system identification. It can be also observed from Fig. 5 that the model identification is pretty good and the hypothesis of LTI model for the magnetic TMD can be considered.

A set of system identifications was carried out to know the relationship between the damping ratio and distance between the magnet and the moving plate. Table 1 shows the identification of the magnetic TMD shown at Fig. 1, denoted as 1^{st} TMD.

3 GENERAL CONTROL STRATEGY

The state space model of the two storey building defined at Eqs. (6) and (7) and the transfer function of the magnetically damped TMD defined at Eq. (12) can be joint in a closed control loop (see Fig. 6). Note that the output force of each TMD is one of the inputs of the building. In addition, the input of each TMD is the output measured with one accelerometer placed at each floor.

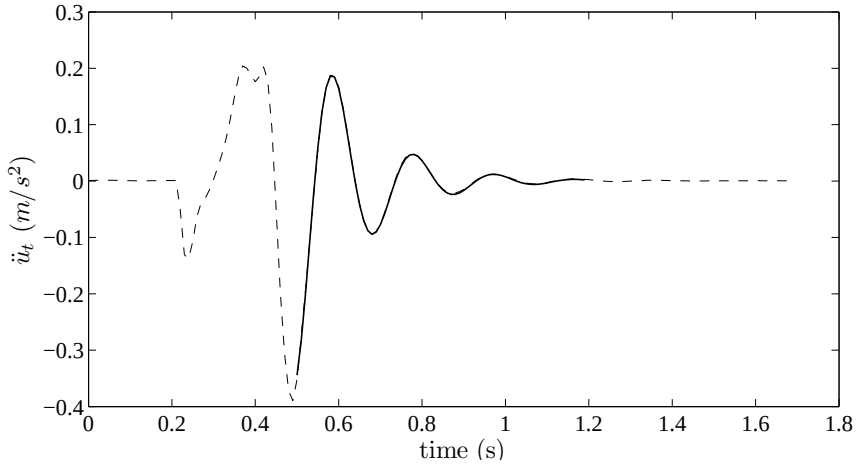

Figure 5: TMD identification example. (−−) time response of the TMD when an impact is applied to the tip mass. (—) Output of the system model when the identified initial conditions are considered.

The general control scheme of Fig. (6) also includes the acceleration of the base (a_b) and the parameters α_{11}, α_{12}, α_{21} and α_{22}. This parameters allow us to place the j^{th} TMD on i^{th} floor ($\alpha_{ij} = 1$). That is, if the configuration is TMD_1 at second floor and TMD_2 at first floor, the values are $\alpha_{11} = 0$, $\alpha_{12} = 1$, $\alpha_{21} = 1$ and $\alpha_{22} = 0$. Note that any TMD cannot be placed in both floors at the same time. Therefore, the variables α_{ij} are treated as boolean variables satisfying the constraints $\alpha_{11} + \alpha_{21} = 1$ and $\alpha_{12} + \alpha_{22} = 1$, which are defined in the optimal control designs.

4 OPTIMAL CONTROL DESIGN METHODOLOGY

The optimal control design methodology consists on considering the TMDs as a closed loop control problem (like in [13]). In this work, two design criteria are considered. The first one finds the value of the vector $\mathbf{V} = [\alpha_{11}, \alpha_{12}, \alpha_{21}, \alpha_{22}, \omega_{t,1}, \omega_{t,2}, \xi_{t,1}, \xi_{t,2}]$ that minimizes the acceleration of one floor (i.e., minimize the value of H_∞ norm of the FRF between y_i and a_b). The second one finds the optimal value of $\mathbf{V}$ that minimizes the maximum of the mode shapes of one vibration mode (i.e., the maximum value of $\boldsymbol{\phi}_i$).

The minimization is carried out by using the built-in function *fminsearch* of MATLAB. The file containing the objective function considers the four possible combinations of α_{ij} to find the optimal values of$[\omega_{t,1}, \omega_{t,2}, \xi_{t,1}, \xi_{t,2}]$ which minimize, as mentioned, the H_∞ norm or the maximum value of $\boldsymbol{\phi}_i$. In addition, the values of $m_{t,1}$ and $m_{t,2}$ are defined because the part (2) of each TMD (see Fig. 1 right) is fixed. In addition, the value of the objective variable is penalized when $[\omega_{t,1}, \omega_{t,2}, \xi_{t,1}, \xi_{t,2}]$ cannot be implemented in practice (i.e., maximum values for $\xi_{t,1}, \xi_{t,2}$ and non negative values for $\omega_{t,1}$, $\omega_{t,2}$, $\xi_{t,1}$ and $\xi_{t,2}$).

ω_t (rad/s)	ξ_t	$\dot{u}_t(0)$ (m/s)	$u_t(0)$ (m)
11.2586	0.0406	0.0005	-0.0041
11.2548	0.0457	0.0042	-0.0045
11.2793	0.0566	0.0040	0.0330
11.2670	0.0672	-0.0374	0.0031
11.2727	0.0811	-0.0400	0.0340
11.2697	0.0981	-0.0312	0.0035
11.2937	0.1221	-0.0423	0.0035
11.2953	0.1538	-0.0348	0.0031
11.4047	0.2320	-0.0278	0.0046
11.5069	0.3143	-0.0273	0.0043
11.3660	0.5147	-0.0304	0.0047

Table 1: System identification of the device TMD_1 shown at Fig. 1.

5 SIMULATION AND EXPERIMENTAL RESULTS

This section show an example of the design explained in Section 4. The values of $m_{t,1}$ and $m_{t,2}$ are fixed in 0.107 kg and 0.072 kg respectively. In addition, the model defined in Eqs. (6) and (7) is updated for the four possible configurations of α_{11}, α_{12}, α_{21} and α_{22} to include the weight of the frame (part (4)) of each TMD. The algorithm can offer several "good configurations" depending on the success of the fminsearch function.

When minimizing the H_∞ norm of the FRF between the acceleration of the second floor (y_2) and the acceleration of the ground (a_b), two (local) solutions are $\alpha_{11} = 0$, $\alpha_{12} = 1$, $\alpha_{21} = 1$ and $\alpha_{22} = 0$ (i.e., TMD_1 placed at second floor and TMD_2 placed at first floor) and $\alpha_{11} = 0$, $\alpha_{12} = 1$, $\alpha_{21} = 0$ and $\alpha_{22} = 1$ (i.e., both TMDS placed at the second floor). The simulation results for both designs are shown in Figs. 7 and 8. The values of TMDs parameters are: i) $\omega_{t,1} = 11.38$ rad/s, $\omega_{t,1} = 32.32$ rad/s, $\xi_{t,1} = 0.0595$ and $\xi_{t,2} = 0.0503$ for Design 1 and ii) $\omega_{t,1} = 10.71$ rad/s, $\omega_{t,1} = 23.29$ rad/s, $\xi_{t,1} = 0.0598$ and $\xi_{t,2} = 0.0525$ for Design 2, which can be implemented in practice. Note that the maximum value of the FRF between y_2 and a_b (i.e., H_∞) is approximately the same for both designs (about 19.4 dB in Fig. 8). Note that the reduction achieved with TMDs is approximately 16 dB in simulation (i.e., the acceleration of the second floor with TMDs is 6.3 time less than without them). However, Fig. 7 shows that Design 2 is worse than Design 1 for the first floor. Since the maximum acceleration measured at first floor of Design 2 is approximately 20 dB, which is bigger than the second floor at both designs, Design 1 is implemented in practice to compared simulation and experimental results.

Figs. (9) and (10) show the FRF between y_1 and a_b and between y_2 and a_b, respectively for Design 1. Note that simulation and experimental results are practically the same, which validate the models and the experimental identifications of the building and TMDs.

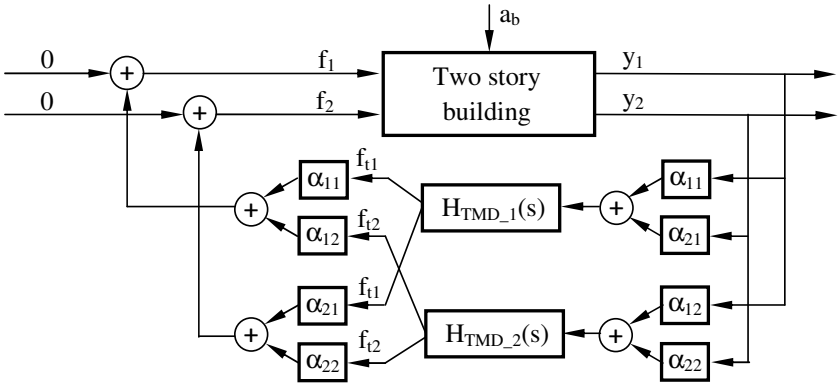

Figure 6: General control scheme.

6 CONCLUSIONS

Using simple TMD prototypes, in which the moving mass is guided by a flexible supporting plate (contact-free) and the damping is trusted to friction-free magnetic effect, enables the possibility to make accurate testing with TMDs and to validate theoretical models.

The results shown in this work validate the laboratory prototype of magnetically damped TMD built in CARTIF (Spain) as a PVC system. In addition, the design methodology simplifies the tuning of the parameters and allows to use it for more complex designs as the AVC implemented at [14].

Future works will be the application of these magnetically damped TMDs to more complex structures, where the control theory can be used to improve the performance of a set of TMDs applied to structures with natural frequencies spatially distributed and closely spaced. In addition, the definition of the functional (i.e., variables to be minimized) must be deeply studied in order to consider the maximum vibration level on the overall structure.

ACKNOWLEDGMENT

The authors wish to acknowledge to the partial support throught Research Projects BIA2011-28493, DPI2013-47441 and BIA2014-59321 (“Ministerio de Economía y Competitividad”, Spanish Government).

REFERENCES

[1] G. Housner, L. Caughey, T. Chassiakos, R. Claus, S. Masri, R. Skelton, T. Soong, B. Spencer, J. Yao, Structural control: Past, present, and future, Engineering Mechanics-ASCE 123 (9) (1997) 887–971.

[2] M. Symans, M. Constantinou, Semi-active control systems for seismic protection of structures: a state-of-the-art review, Engineering Structures 21 (6) (1999) 469–487.

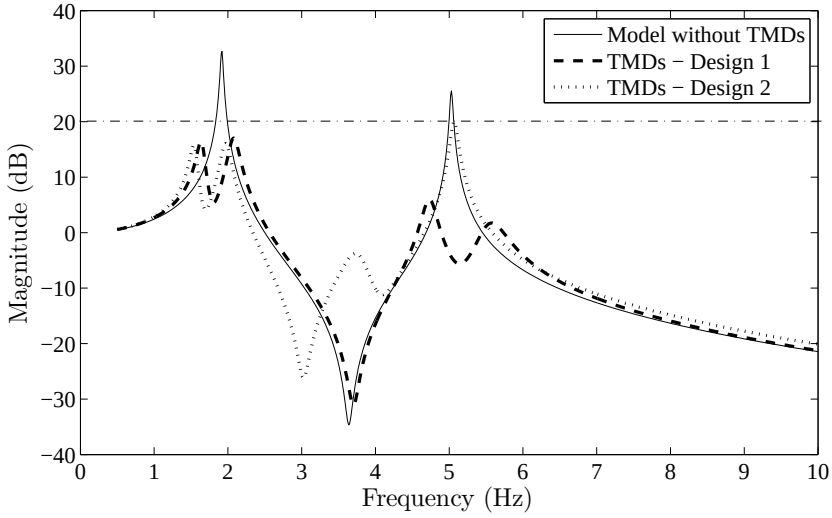

Figure 7: TMDs design. Simulation results for first floor.

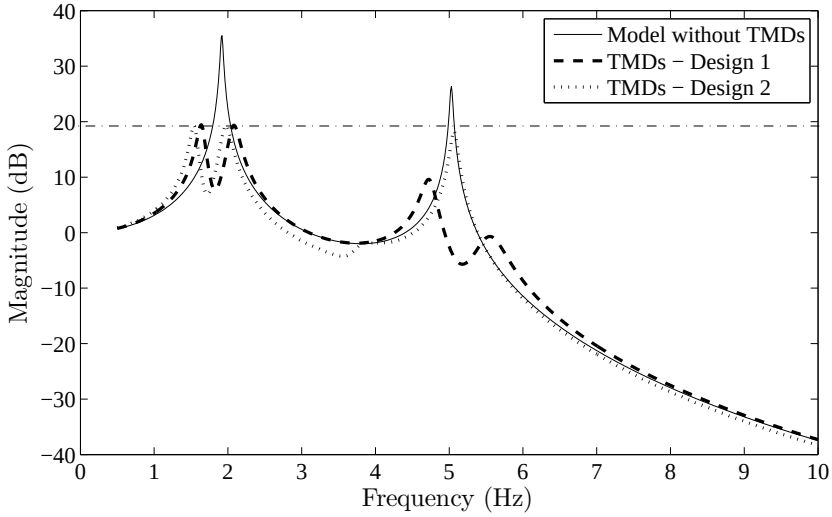

Figure 8: TMDs design. Simulation results for second floor.

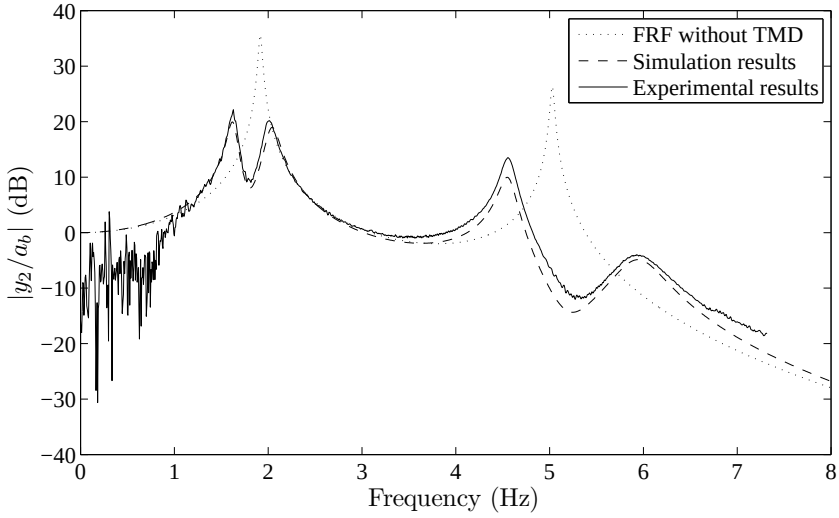

Figure 9: Simulation and experimental results for the first floor (Design 1).

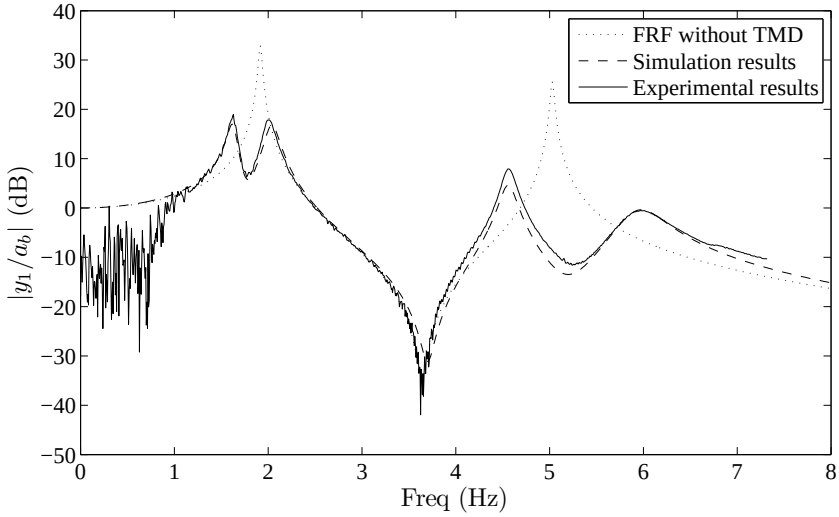

Figure 10: Simulation and experimental results for the second floor (Design 2).

[3] F. Bourquin, G. Caruso, M. Peigney, D. Siegert, Magnetically tuned mass dampers for optimal vibration damping of large structures, Smart Materials and Structures 23 (8) (2014) 085009.

[4] Z. Wang, Z. Chen, Development and performance tests of an eddy-current tuned mass damper with permanent magnets, Journal of Vibration Engineering 26 (3) (2013) 374–379.

[5] C. Sun, S. Nagarajaiah, A. Dick, Family of smart tuned mass dampers with variable frequency under harmonic excitations and ground motions: closed-form evaluation, Smart Structures and Systems 13 (2) (2014) 319–341.

[6] M. Berardengo, A. Cigada, F. Guanziroli, S. Manzoni, Modelling and control of an adaptive tuned mass damper based on shape memory alloys and eddy currents, Journal of Sound and Vibration 349 (2015) 13–38.

[7] J. P. Den-Hartog, Mechanical Vibrations, New York: McGraw-Hill, 1956.

[8] M. Abe, T. Igusa, Tuned mass dampers for structures with closely spaced natural frequencies, Earthquake Engineering and Structural Dynamics 24 (1995) 247–261.

[9] R. Greco, A. Lucchini, G. Marano, Robust design of tuned mass dampers installed on multi-degree-of-freedom structures subjected to seismic action, Engineering Optimization 47 (8) (2015) 1009–1030.

[10] L. Fleck-Fade-Miguel, L. Fleck-Fadel-Miguel, R. Holdorf-Lopez, Robust design optimization of friction dampers for structural response control, Structural Control and Health Monitoring 332 (9) (2014) 6044–6062.

[11] A. D. N. Debnath, S. K. Deb, Frequency band-wise passive control of linear time invariant structural systems with h-infinity optimization.

[12] http://www.quanser.com, consulted at January 2016.

[13] A. Mohtat, E. Dehghan-Niri, Generalized framework for robust design of tuned mass damper systems, Journal of Sound and Vibration 330 (5) (2011) 902–922.

[14] E. Pereira, I. M. Díaz, E. J. Hudson, P. Reynolds, Optimal control-based methodology for active vibration control of pedestrian structures, Engineering Structures 80 (1) (2014) 153–162.